# Truncation of a β-Barrel Scaffold Dissociates Intrinsic Stability from Its Propensity to Aggregation

Lucrecia M. Curto,[†] Carla R. Angelani,[†] Julio J. Caramelo,[†] and José M. Delfino[†*]
[†]Department of Biological Chemistry and Institute of Biochemistry and Biophysics, School of Pharmacy and Biochemistry, University of Buenos Aires, Buenos Aires, Argentina

ABSTRACT Δ98Δ is a functional all-β sheet variant of intestinal fatty acid binding protein (IFABP) that was generated by controlled proteolysis. This framework is useful to study the molecular determinants related to aggregation of β-barrel proteins. Albeit displaying increased conformational plasticity, Δ98Δ exhibits a nativelike β-barrel topology and is able to support a cooperative folding behavior. Here we present a comparative study of IFABP and Δ98Δ regarding their conformational perturbation and aggregation propensity triggered by trifluoroethanol. Both proteins share a common nucleation-elongation mechanism, whereby the rate-limiting step is the formation of stable dimeric nuclei followed by the association of monomers to the growing aggregates. Despite leading to a less stable structure, the extensive truncation of IFABP yields a form exhibiting a somewhat lower tendency to aggregate. This finding appears at odds with the established notion that a perturbation of the native compact fold should necessarily favor the population of aggregation-prone species. In addition to the aggregation propensity dictated by a given amino-acid sequence, our contention holds that long-range interactions might also play a major role in determining the overall aggregation propensity.

## INTRODUCTION

Despite the low-sequence identity displayed by the members of the fatty acid binding protein (FABP) family, FABPs share a similar β-barrel fold that resembles a clamshell. In particular, intestinal fatty acid binding protein (IFABP) is a 131-amino-acid monomeric β-barrel protein consisting of two five-stranded β-sheets (βA-βE and βF-βJ). These sheets are arranged in a nearly orthogonal orientation enclosing the ligand-binding cavity. All β-strands are connected by β-turns with the exception of strands βA and βB, where an intervening helix-turn-helix motif appears (Fig. 1). This structure differs from most globular proteins because its interior is occupied by a large solvent-filled cavity, whereas the hydrophobic core is small and displaced from the protein center. By using proteolysis with the enzyme Arg-C, a natural tool sensitive to local flexibility, we recently generated two all-β-sheet abridged variants of IFABP: Δ98Δ (1,2) and Δ78Δ (3). (Specifically, Δ98Δ is a truncated variant of IFABP corresponding to the fragment 29–126 of the parent protein.)

Even though Δ98Δ lacks one-quarter of the sequence of the parent protein (98 amino acids, encompassing residues 29–126 of IFABP), it is able to fold into a monomeric structure retaining functional activity. By comparison with the full-length protein, Δ98Δ is devoid of βA, most of the helical motif, and the last five amino acids belonging to the C-terminal β-strand (Fig. 1). Most significantly, this truncation leads to the loss of both stretches implicated in the closure of the β-barrel. In IFABP, this region comprises a hydrogen-bonding network involving residues of the distal part of strands βA and βJ, which belong to different β-sheets. The temperature or GdnHCl-induced equilibrium unfolding of Δ98Δ displays a cooperative transition, albeit less pronounced than that observed for IFABP. In addition, lower transition midpoints indicate that the abridged variant is less stable than the parent protein. Nevertheless, the bulk of evidence suggests that Δ98Δ preserves a small cooperative nucleus able to support a nativelike β-barrel scaffold (2).

There are few β-class proteins useful as model systems for protein engineering, mainly due to their high tendency to aggregate. For instance, the design of monomeric all-β domains such as betabellin (4) and betadoublet (5) yielded species similar to molten globule intermediates. In this regard, the generation of truncated variants of IFABP that retain key structural and functional attributes allows the exploration of those determinants underlying conformational change and aggregation. It is noteworthy that even though Δ98Δ might display free edges, it shows no tendency to aggregate spontaneously (2). Because the presence of β-sheet elements is central to amyloid structure, naturally occurring β-sheet proteins usually avoid potentially dangerous edge-to-edge interactions (6). In this context, Δ98Δ becomes a useful model to explore the critical elements leading to β-aggregates.

The effect of alcohols on native proteins and unfolded peptides has been studied extensively. In particular, 2,2,2-trifluoroethanol (TFE) has often been chosen for such studies because of its ability to induce helical structures in

*Submitted January 12, 2012, and accepted for publication September 5, 2012.*

*Correspondence: delfino@qb.ffyb.uba.ar

Julio J. Caramelo's present address is Instituto de Investigaciones Bioquímicas de Buenos Aires-CONICET and Laboratory of Structural Cell Biology, Leloir Institute Foundation, and Department of Biological Chemistry-School of Sciences-University of Buenos Aires, Buenos Aires, Argentina.

Editor: Heinrich Roder.


0006-3495/12/11/1929/11 $2.00

http://dx.doi.org/10.1016/j.bpj.2012.09.002

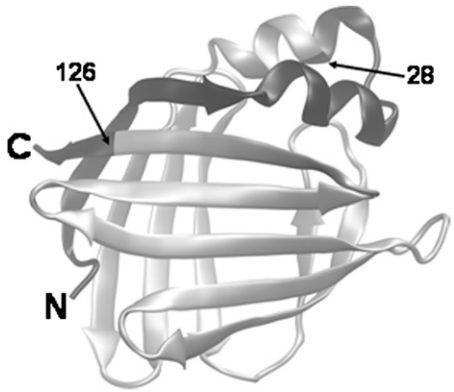


FIGURE 1 Ribbon structure of IFABP (PDB:2IFB). (*Shaded*) Δ98Δ construct, and (*solid*) excised N- and C-termini stretches (1–28 and 126–131, respectively).

peptides and to denature the native structure of proteins (7). The most important factor for the observed effect has been attributed to the decrease in the hydrophobic interactions. In aqueous solutions of water-miscible fluorinated alcohols at intermediate concentrations, i.e., at ~30% v/v, alcohol molecules associate so as to minimize their contact with water. This results in the formation of micellelike clusters with the hydrophobic groups located inside, although no macroscopic phase separation takes place. Such clusters of alcohol molecules provide a highly hydrophobic local environment where polarity decreases.

This low polarity weakens the hydrophobic interactions that stabilize the compact native structure of proteins, but simultaneously strengthens electrostatic interactions such as hydrogen bonds, thus stabilizing secondary structures, particularly the $\alpha$-helix. Upon binding to these hydrophobic clusters, proteins and peptides undergo a conformational transition, as they do upon binding to SDS micelles. At higher concentration of alcohols, the micellelike clusters disappear, resulting in a homogeneous solution (7). Due to its ability to promote conformational transitions leading to nonnative states, TFE was widely used to trigger protein aggregation or amyloid formation (8–12). Intermediate levels of the cosolvent TFE promote the conversion of proteins into nativelike aggregation-prone species. The occurrence of this early perturbation step means that global unfolding may not necessarily represent a prerequisite for the initiation of aggregation (8).

Here we present a comparative study of the conformation and aggregation propensity of IFABP and Δ98Δ—an abridged all-$\beta$ sheet variant of this protein—occurring upon the structural perturbation exerted by TFE. Having in mind that

1. Δ98Δ shares an amino-acid sequence identical to a major central part of IFABP,
2. it might expose free edges, and
3. it adopts a less stable nativelike structure,

it is tempting to predict an accelerated rate of aggregation for this variant. Contrary to expectation, Δ98Δ displays a similar (or even lower) tendency to aggregate. These frameworks illustrate the complexity and risks in attempting to understand protein aggregation exclusively on the basis of characteristic sequence motifs. This study reveals that this phenomenon would not solely be dictated by the presence or absence of contiguous amino-acid stretches, but the interpretation should necessarily include the role played by long-distance interactions.

## MATERIALS AND METHODS

### Materials

Rat IFABP cDNA, coded in the plasmid pET-11a, was expressed in *Escherichia coli* strain BL21(DE3) and the protein was purified as described previously (13). Recombinant Δ98Δ cDNA coded in the plasmid pET-22b(+) was expressed in *E. coli* strain BL26 and the protein was purified as described previously (2). The chemicals 2,2,2-trifluoroethanol (TFE), Thioflavin-T (Th-T), Congo Red (CR), and buffers were purchased from Sigma-Aldrich (St. Louis, MO). All solutions were made in 5 mM sodium phosphate buffer, 150 mM NaCl, pH 8.0.

Peptide 1–28, AFDGTWKVDRNENYEKFMEKMGINVVKR, was synthesized and partially purified up to the desalting step by GenScript (Piscataway, NJ). The purification was completed by HPLC using a reverse phase C4 semipreparative column (Cat. No. 214TP510; Grace Vydac, Hesperia, CA) equilibrated in 0.05% v/v aqueous trifluoroacetic acid. The peptide was eluted with a linear gradient from 0 to 80% v/v aqueous acetonitrile, 0.05% v/v trifluoroacetic acid. The fraction eluting at ~45% v/v acetonitrile, containing pure peptide, was lyophilized. The covalent structure of this peptide was verified by matrix-assisted, laser-desorption-ionization-time-of-flight mass spectrometry at the local protein facility (LANAIS-PRO, the University of Buenos Aires-Consejo Nacional de Investigaciones Científicas y Técnicas (CONICET)).

Protein and peptide concentration was estimated by ultraviolet (UV) absorption: $\varepsilon_{280nm}$ = 15,910, 9154, and 6756 $M^{-1}$ $cm^{-1}$ for IFABP, Δ98Δ, and peptide 1–28, respectively.

For end-point protein aggregation measurements, samples were incubated at a given TFE concentration for at least 2 h, a time sufficient to attain a stable turbidity reading. To avoid fragmentation of the fibrils, no stirring was applied (14). Unless otherwise stated, the final concentration of protein and TFE is 0.24 mg $mL^{-1}$ and 25% v/v, respectively.

### Dye binding assays

Th-T and CR binding assays were performed according to Nilsson (15). Briefly, for the Th-T assay, 20 $\mu$L of protein samples (0.24 mg $mL^{-1}$) incubated for 2 h at the concentrations of TFE shown were diluted in 2 mL of Th-T solution. The fluorescence intensity of this solution (position of the maximum wavelength of fluorescence emission, $\lambda_{max}$, 482 nm) is subtracted from that of a protein sample at 0% v/v TFE (that in turn results equal to a sample without protein). For the CR assay, the wet protein pellets obtained after centrifugation of samples incubated for 2 h at the concentrations of TFE shown (5 $\mu$L) were diluted in 1 mL of CR solution. The absorbance at 540 nm of each solution is subtracted from that of a sample without protein.

For polarized light microscopy, TFE-aggregated proteins dried onto coverslips were stained with CR and observed under polarized light, also following the procedures described by Nilsson (15).

### Circular dichroism

Spectra were recorded on a model No. J-810 spectropolarimeter (JASCO, Easton, MD). Data in the near-UV (250–320 nm) or in the

far-UV (200–250 nm) regions were collected at 25°C using a 10- or a 1-mm-pathlength cuvette, respectively. A scan speed of 20 nm $min^{-1}$ with a time constant of 1 s was used for both proteins. Each spectrum was measured at least three times and the data was averaged to minimize noise. Molar ellipticity was calculated as described elsewhere (16), using a mean-residue-weight value of 114.4 and 112.0 for IFABP and Δ98Δ, respectively.

## Fluorescence measurements

Fluorescence measurements were performed at 25°C in a model No. FP-6500 spectrofluorimeter (JASCO) equipped with a thermostated cell. A 3-mm path cuvette sealed with a Teflon cap was used. The intrinsic emission spectra were obtained in the absence or presence of appropriate concentrations of TFE. In this case, excitation wavelength was 295 nm and emission was collected in the range 310–410 nm. The excitation and emission monochromator slit widths were both set at 5 nm. For each spectrum, the total integrated intensity and the maximum wavelength of fluorescence emission ($\lambda_{max}$) were the parameters used for further analysis.

## Transmission electron microscopy

Samples containing 0.24 mg $mL^{-1}$ of IFABP or Δ98Δ in 25% v/v TFE were incubated overnight. The following day, pellets were resuspended in 20 mM Tris-HCl buffer at pH 8.0. A 5-μL sample was placed on carbon-coated copper grids, and allowed to stand for 2 min. The grids were then washed with distilled water and stained with 2% w/v uranyl acetate for an additional 2-min period. Images were taken with a model No. EM 301 transmission electron microscope (Philips Electron Optics, Eindhoven, The Netherlands) located at the Center for Advanced Microscopies (School of Sciences, University of Buenos Aires, Buenos Aires, Argentina).

## Aggregation kinetics

The extent of aggregation was followed by the evolution of turbidity at 350 nm ($A_{350nm}$) on a model No. J-550 spectrophotometer (JASCO). Samples containing IFABP (0.05–0.87 mg $mL^{-1}$, 3.6–58.3 μM) or Δ98Δ (0.04–0.54 mg $mL^{-1}$, 3.3–48.7 μM) in 25% v/v TFE were measured at 25°C. A fixed amount of neat TFE (213 μL) was added to the protein solution (637 μL) and the content was mixed immediately by inverting the cuvette three times before beginning the collection of turbidity readings. The whole procedure does not represent a delay >10 s, an acceptable dead-time for kinetic measurements in a timescale of minutes. Here again, no stirring was ever applied to samples, due to its known effect on fibril fragmentation (14).

All kinetic data describing the aggregation process share a similar sigmoid shape (see Fig. 3 and Fig. S1 in the Supporting Material). As such, they were found to comply with the phenomenological scaling (17), meaning that a single function $f$ is able to describe all time courses. In mathematical terms, this can be stated as follows: $A/A_{lim} = f[t/t_{char}]$, where $A_{lim}$ is the limiting value of the turbidity as time tends to infinity while $t_{char}$ is a characteristic time for the process. The implication of satisfying this scaling property is that all kinetics share the same assembly pathway.

Independently, an empirical model (18) was fitted to the measured turbidity as a function of time. Here, the aggregation process is considered an irreversible reaction starting with the association of $n$ molecules of non-aggregated protein P,

$$nP \xrightarrow{k_n} P_{agg},$$

where $P_{agg}$ is the aggregated form and $k_n$ is the $n^{th}$ order rate constant. The rate of aggregation may be written as the time-dependent decay of the non-aggregated protein concentration ($v_{agg} = -d[P]/dt$). Because the turbidity of the protein solution is assumed to be proportional to the amount of aggregated protein, i.e., $A \propto [P_{agg}]$, the evolution of turbidity with time follows the expression

$$\frac{dA}{dt} = k(A_{\lim} - A)^n, \tag{1}$$

where $A$ is the turbidity at time $t$; $A_{lim}$ is the limiting value of the turbidity as time tends to infinity; and $k = nk_n[P]_0^{n-1}/A_{\lim}^{n-1}$, in which $[P]_0$ is the initial (total) protein concentration. When $n = 1$ (first-order process of aggregation with respect to protein), Eq. 1 becomes

$$\frac{dA}{dt} = k_1(A_{\lim} - A), \tag{2}$$

where $k_1$ is the first-order rate constant. Integration of Eq. 2 gives the expression describing the expected dependence of $A$ on $t$,

$$A = A_{\lim}\left\{1 - e^{[-k_1(t-t_0)]}\right\}, \tag{3}$$

where $t_0$ is a lag time during which $A \simeq 0$. The model was fitted to the data by nonlinear regression analysis using the Microsoft Excel solver tool (Microsoft, Redmond, WA). The agreement between the experimental data and the calculated values was estimated by the $R^2$ correlation coefficient (18).

# RESULTS

## TFE-induced aggregation of proteins

Turbidity at 350 nm of IFABP and Δ98Δ incubated at various TFE concentrations was measured (Fig. 2). In the absence of TFE, there is no evidence of aggregation, not even after incubation of each protein at 50°C for 6 h (data not shown). At intermediate TFE concentrations (20–55% v/v), both proteins exhibit a similar increment in the turbidity, indicating the occurrence of an aggregation process. More precisely, in both cases a maximum value was found at ~25% v/v TFE. In view of these facts, the time-course measurement of the turbidity was recorded at various protein concentrations (Fig. 3, *A* and *B*). An evident common feature is the sigmoidicity of the kinetics,

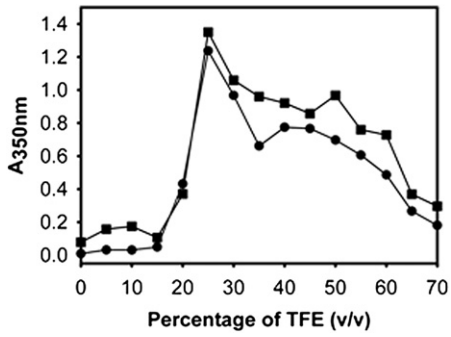


FIGURE 2 TFE-induced aggregation of proteins. Turbidity at 350 nm of IFABP (■) and Δ98Δ (●) solutions (0.24 mg $mL^{-1}$) was measured at increasing concentrations of TFE. After incubation for 2 h, i.e., until a stable reading is reached, each sample was transferred to the cuvette, yielding a homogeneous suspension.

characterized by the occurrence of a concentration-dependent lag period before the onset of aggregation (see also Fig. S1 and the ensuing analysis described below).

To test the notion that the missing regions in Δ98Δ with respect to IFABP might include key determinants relevant for aggregation, the major excised stretch (peptide 1–28) was synthesized and tested alongside Δ98Δ in its ability to influence this process (Fig. 3 *C*). In isolation, peptide 1–28 shows no tendency whatsoever to form TFE-induced aggregates. Consistently, incubation of this peptide in buffer for 6 h at 50°C does not bring about aggregation either (data not shown). In addition, an equimolar mixture of the latter with Δ98Δ, preincubated for 1 h at room temperature before the addition of TFE, exhibits the same aggregation behavior as pure Δ98Δ.

The aggregation kinetics was analyzed by plotting the scaled turbidity ($A/A_{lim}$, where $A_{lim}$ is the asymptotic value of turbidity measured at a given protein concentration) against the scaled time ($t/t_{1/2}$, where $t_{1/2}$ is the characteristic time needed for the turbidity to reach half the value of $A_{lim}$). Interestingly, at all protein concentrations the scaled curves measured for IFABP and Δ98Δ fall into a single curve (Fig. 3 *D*, but compare to Fig. 3 in Flyvbjerg et al. (17)), suggesting a common underlying aggregation mechanism. Likewise, the kinetics corresponding to the mixture Δ98Δ/peptide 1–28 overlaps with the former, indicating the lack of any influence of the peptide on the aggregation process of the abridged form.

When assayed at 45% v/v TFE, both proteins increase the time needed to reach the turbidity plateau. In this experimental condition, Δ98Δ also displays a higher $t_{1/2}$ than the full-length protein, indicating a lower rate of aggregation for the truncated variant (data not shown). Furthermore, the scaled curves at 45% v/v TFE show less sigmoidicity than those measured at 25% v/v TFE (see Fig. S2).

To further investigate the aggregation mechanism at 25% v/v TFE, the Wang and Kurganov model (18) was fitted to the data. The aggregation curves from $A/A_{lim} \sim 0.1$ to higher values are satisfactorily described by a pseudo-first-order kinetics (Eq. 2, $R^2 > 0.997$). This is inferred from the linear dependence of the rate constant $k_1$ with protein concentration (Fig. 4 *A*). Additionally, this procedure allows the determination of parameters $A_{lim}$ (Fig. 4 *B*) and $t_0$ (lag time, Fig. 4 *C*). The latter displays an inverse hyperbolic dependence with total protein concentration. For both proteins, $A_{lim}$ values are similar and proportional to total protein concentration, suggesting that the turbidity value faithfully reflects the extent of protein aggregation. Assuming that at $t \geq t_0$, aggregation follows a first-order kinetics, the rate of this process may be calculated as the slope of a tangent to the curve at $t \simeq t_0$ (mathematically equivalent to the product $A_{lim}\, k_1$).

Because both $A_{lim}$ and $k_1$ were found to depend linearly on protein concentration, this product will be proportional to the square of protein concentration (Fig. 4 *D*), a fact indicative of a second-order kinetics. From the slope of these curves, Δ98Δ shows a twofold decrease in the rate of aggregation, as compared to IFABP. Under the assumption that the concentration of nuclei remains constant during the elongation phase, the second-order association reaction can be satisfactorily described by an apparent first-order kinetics. This is consistent with the sequential protein monomer addition to preformed nuclei. In summary, the common features of the TFE-induced aggregation kinetics of IFABP and Δ98Δ are:1. the existence of a lag period, 2. the inverse dependence of this lag period with protein

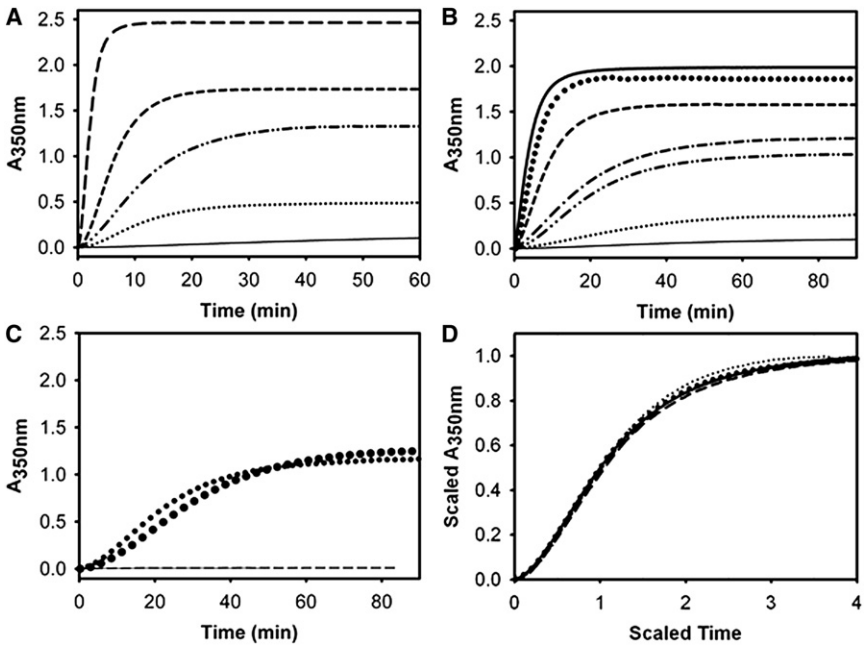


FIGURE 3 Kinetics of aggregation of proteins. Effect of concentration on the kinetics of aggregation at 25% v/v TFE, as followed by measuring turbidity at 350 nm of IFABP (*A*) at 3.6 (*solid line*), 9.3 (*small dotted line*), 16 (*dash-dot-dot-dash line*), 29.2 (*short-dashed line*), 58.3 μM (*long-dashed line*); Δ98Δ (*B*) at 3.3 (*solid line*), 9.3 (*small dotted line*), 16 (*dash-dot-dot-dash line*), 21.6 (*dash-dot-dash line*), 29.4 (*short dashed line*), 40.6 (*large dotted line*), 45.1 μM (*solid thick line*); and peptide 1–28 (*C*) at 29 μM (*solid line*), 58 μM (*short-dashed line*), and in the presence of Δ98Δ at 29 μM (*small dotted line*); pure Δ98Δ at this same concentration (*large dotted line*) is shown alongside for comparison. (*D*) Replot of the data shown in panel *A* (*continuous lines*), panel *B* (*dashed lines*), and panel *C* (*dotted lines*) after scaling turbidity ($A/A_{lim}$) and time ($t/t_{1/2}$).

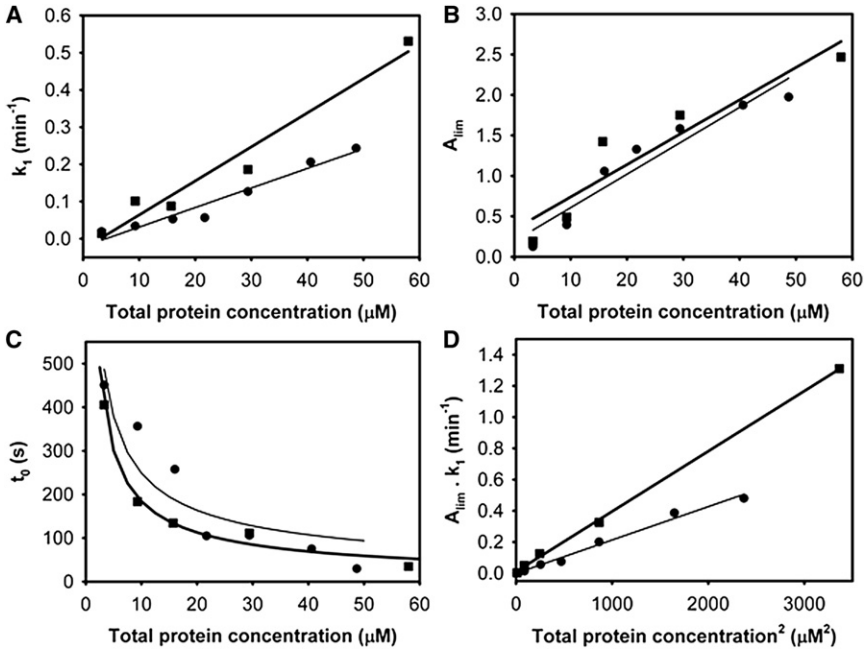


FIGURE 4 Protein concentration dependence of kinetic parameters. For IFABP (■) and Δ98Δ (●), the dependence on total protein concentration of the rate constant $k_1$ (*A*), $A_{lim}$ (*B*), and the lag time $t_0$ (*C*) are shown. (*D*) Rate of aggregation at $t = t_0$ (equal to the product $A_{lim}$ $k_1$) as a function of the concentration of protein squared.

concentration, and 3. the second-order of this process with respect to protein concentration.

Independently, one can follow the phenomenological formalism put forward by Flyvbjerg et al. (17) to analyze kinetic data. For the earliest times, i.e., for $t \simeq 0$, the relationship holds that

$$A \propto t^{k+2}, \tag{4}$$

where $k$ is the number of intermediate assembly steps of nucleus $P^*_n$ (see Scheme 1, and compare to Eq. 14 in Flyvbjerg et al. (17)):

$$P \rightleftarrows P^* \xrightarrow{f_0} P^*_n \underset{P^* \nearrow}{\xrightarrow{f_1}} F. \qquad \text{(SCHEME 1)}$$

In this fashion, the initial slope of a double-log plot of $A/A_{\lim}$ versus $t$ yields an integer value of ~2 (Fig. 5 *A*; but compare to Figs. 2 and 6 in Flyvbjerg et al. (17)), meaning that for both proteins a stable nucleus is created in one step, i.e., $k = 0$. Furthermore, the following simple inverse relationship was also found, as

$$t_{1/2} \propto A_{\lim}^{-s}, \tag{5}$$

where $s \sim 1$, as shown in a double-log plot of these variables (but compare to Eq. 3 in Flyvbjerg et al. (17), and see our Fig. 5 *B*, but compare to Fig. 4 in Flyvbjerg et al. (17)). Like the scaling property, this indicates that a single mechanism accounts for the observed assembly reaction. Furthermore, because the size $n$ of the nucleus is

$$n = s(k + 2), \tag{6}$$

this imposes a restriction on the kinetic model by which the active nucleus is indeed a dimeric species, i.e., $n \sim 2$ (but compare to Eq. 15 in Flyvbjerg et al. (17)).

In agreement with this view, the irreversible process of protein aggregation can be divided into two steps, where the first is the rate-limiting dimerization giving rise to the nucleus, followed by the sequential association of monomers to the growing fibril (see Scheme 1).

## TFE-induced aggregates display amyloidlike features

The possibility that the aggregates formed displayed amyloidlike properties was examined through their ability to bind amyloid-sensitive dyes and by the inspection of their structural characteristics by microscopy.

Both Th-T and CR interact with the crossed-$\beta$-sheet structure common to a variety of amyloid structures (15). It is well known that upon Th-T binding there is an increase in fluorescence emission (19). For IFABP and Δ98Δ, no appreciable changes were detected in the fluorescence of Th-T up to 15% v/v TFE. By contrast, a sharp increase in the intensity at 482 nm was observed at ~25% v/v TFE (Fig. 6 *A*). Beyond this point, the fluorescence emission intensity decreases in a very similar fashion to the course followed by the turbidity (Fig. 2).

CR binding to proteins can be detected both by an increase in the absorbance and by a red shift of the maximum. These changes can be best quantified by measuring the difference spectrum between those of the free and protein-bound dye. Here again, regardless of small quantitative differences, CR binding to each protein assayed

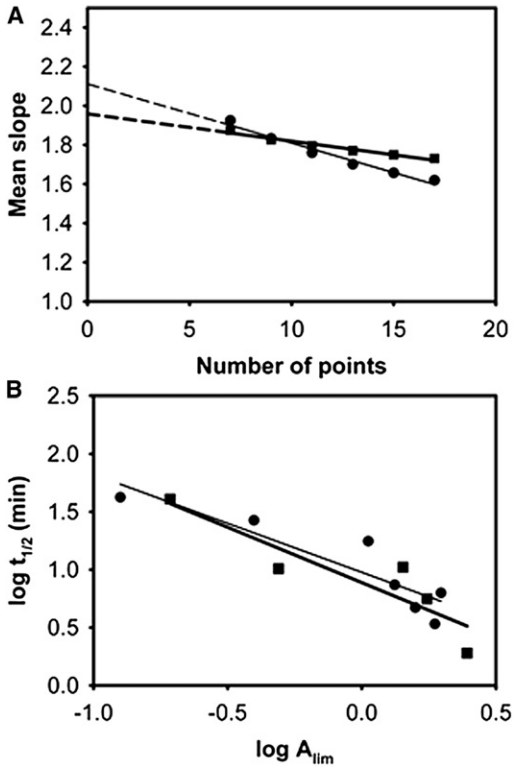


FIGURE 5 Phenomenological parameters of the protein aggregation process. The initial slope (at $t \simeq 0$) of a double-log plot of $A/A_{lim}$ versus time for IFABP (■) and Δ98Δ (●) is plotted in panel *A*. Extrapolation to the first data points of each time series gives an integer value of ~2 for both proteins. (*B*) Double-log plot of the characteristic time $t_{1/2}$ versus $A_{lim}$. The slopes of the fitted curves are 0.95 ± 0.26 and 0.85 ± 0.17 for IFABP (■) and Δ98Δ (●), respectively.

displays a maximum centered at 25% v/v TFE (Fig. 6 *B*). At the highest concentrations of TFE assayed (60–70% v/v), the absorbance of each sample was considerably higher than that measured for subaggregating conditions (e.g., up to 15% v/v). Consistently, at these low TFE concentrations, no significant red shift occurs (data not shown).

Furthermore, aggregates of both IFABP and Δ98Δ formed in 25% v/v TFE stained with CR exhibit yellowish-green birefringence when examined under polarized light, a characteristic feature of amyloid fibrils (Fig. 7). The micrographs obtained by transmission electron microscopy of these samples are shown in Fig. 8. Although mature fibril morphology is not clearly apparent, annular and several rodlike structures exhibiting different lengths and curvatures are present, features also indicative of fibrillar material.

## Effect of TFE on protein conformation

TFE-induced changes in secondary structure of both proteins were monitored by far- and near-UV circular dichroism spectroscopy. The spectrum of IFABP in buffer shows a positive band centered at ~200 nm and a negative

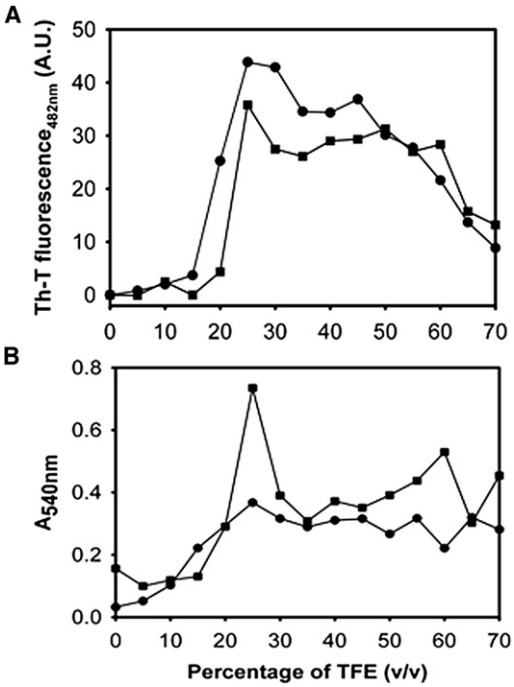


FIGURE 6 Binding of amyloid dyes to the proteins. The fluorescence emission of Th-T (*A*) and the absorbance of CR (*B*) were measured upon binding of the dyes to IFABP (■) or Δ98Δ (●).

band with a minimum at ~216 nm, the latter being a distinctive feature of $\beta$-sheet structure, a character that is kept up to 45% v/v TFE (Fig. 9 *A*). Nevertheless, one should point out

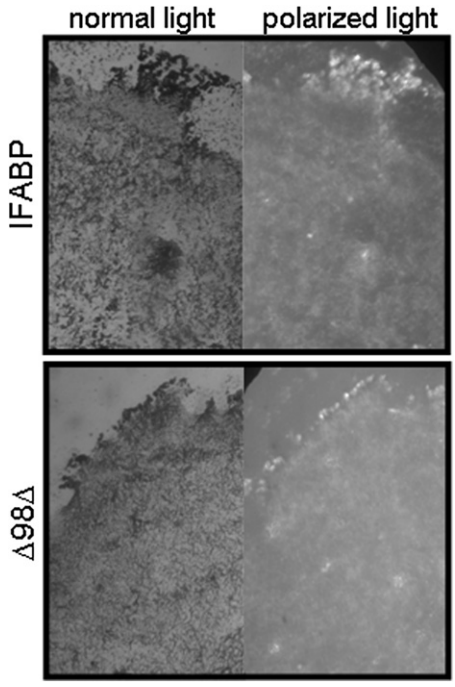


FIGURE 7 Light microscopy images of protein aggregates. Aggregates of IFABP or Δ98Δ stained with CR are shown at 50× magnification under normal or polarized light.

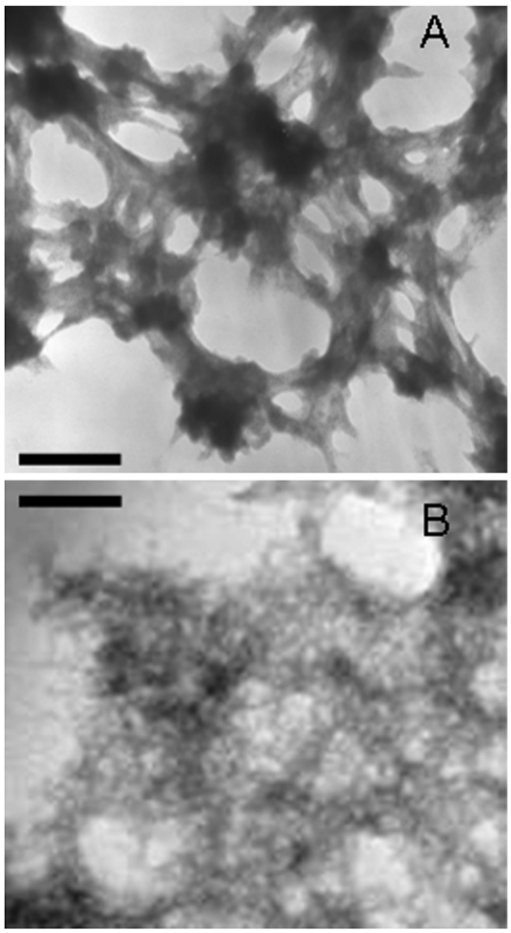


FIGURE 8 Transmission electron microscopy of protein aggregates. Micrographs of IFABP (*A*) and Δ98Δ (*B*) after incubation at room temperature for one day in the presence of 25% v/v TFE are shown. The scale bar represents 200 nm.

the following differences: whereas the spectra at 0 and 15% v/v TFE are almost identical, those taken at 25 and 45% v/v TFE display a ~4-nm red shift of the position of the minimum. The magnitude and the position of the new minimum is typical of largely extended $\beta$-sheet conformation, a structure prevalent in amyloid fibrillar aggregates (12,20). Conversely, at 65% v/v TFE the spectrum of IFABP shows a dramatic change in its shape toward one with two negative bands at ~208 nm and ~222 nm, typical of $\alpha$-helical proteins. The secondary structure content derived from the latter spectrum was calculated with the DICHROWEB server (21,22), using the algorithm Kd2 (23). The comparison against the reference content for native IFABP read from the PDB file (PDB:2IFB) revealed a 4.4-fold decrease in $\beta$-structure (from 71 to 16% v/v), a twofold increase in $\alpha$-helix (from 14 to 27% v/v), and an increment in irregular structure (from 15 to 57% v/v).

The far-UV circular dichroism (CD) spectrum of native Δ98Δ displaying a minimum at ~216 nm is also typical of $\beta$-sheet conformation and, due to the absence of the helical subdomain, the positive band centered at ~200 nm disappears (Fig. 9 *B*, see also Curto et al. (1)). Interestingly, the presence of a subaggregating concentration of TFE (15% v/v) modifies both the shape and the intensity of the spectrum, yielding one that is remarkably similar to that of native IFABP (Fig. 9 *A*). At 25 and 45% v/v TFE, the shape of the spectra remains $\beta$-like, accompanied by a red shift to 220 nm of the main negative band. For the 45% v/v TFE spectrum, an enhancement in the intensity of this dichroic signal is observed. In a manner similar to IFABP, at 65% v/v TFE the far-UV CD spectrum of Δ98Δ displays two negative bands at ~208 nm and ~222 nm. Again, the secondary structure content at this last condition was calculated with the algorithm Kd2, rendering 12% $\beta$-strand, 31% $\alpha$-helix, and 57% disordered structure. Overall, the magnitude of the spectral changes observed points to a higher conformational flexibility of Δ98Δ as compared to the parent protein.

IFABP shows a characteristic near-UV CD spectrum rich in fine structure, whereas Δ98Δ displays bands of lesser magnitude (1). Fig. 9, *C* and *D*, shows that—for both proteins—only slight spectral changes take place by the addition of up to 15% v/v TFE. At 25% v/v TFE and higher cosolvent concentrations, the proteins reveal large deviations from their native spectra (see *insets* to Fig. 9).

IFABP contains two Trp residues: Trp-82, which is buried within the hydrophobic core at the bottom of the ligand binding pocket, and Trp-6 belonging to the N-terminal $\beta$-strand (Fig. 1). Both residues are almost completely occluded from the aqueous solvent (24). We presented evidence that in Δ98Δ the only remaining Trp (Trp-82) is placed in a similar milieu to that in IFABP (2). In the full-length protein, this residue is known to contribute ~75% of the fluorescence emission and there is almost no cross-talk between both Trp residues (25). For these reasons, Trp-82 becomes a useful spectroscopic probe for the hydrophobic core. Taking into account that proteins might retain their native structure in the presence of moderate concentrations of alcohol, TFE was used to probe solvent accessibility of Trp residues due to its ability to quench indole fluorescence by excited-state proton transfer (26). In this sense, changes in Trp fluorescence induced by TFE should be interpreted cautiously, as both the denaturing and quenching effects of TFE can take place concomitantly. In this regard, it was found that in going from an aqueous buffer to 100% v/v TFE, *n*-acetyl-L-tryptophanamide (NATA) exhibits a 3-nm blue shift of its emission peak (from 353 to 350 nm), and a more than fourfold decrease in quantum yield (27).

Similarly, an approximately fivefold decrease of the quantum yield of NATA in 30% v/v TFE as compared to water was measured (28). Fig. 10 shows the evolution of the fluorescence intensity and the position of the maximum wavelength ($\lambda_{max}$) as a function of TFE concentration. From 0 to 20% v/v TFE, $\lambda_{max}$ remains almost invariant (332 nm) for IFABP, despite a significant decrease in the intensity.

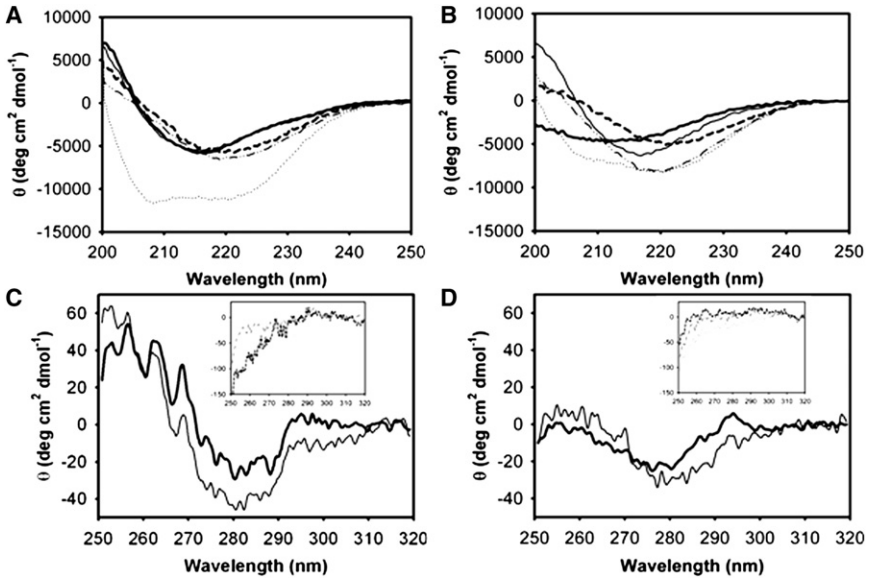


FIGURE 9 Circular dichroism spectroscopy of proteins. CD spectra of IFABP (*A* and *C*) or Δ98Δ (*B* and *D*) at increasing TFE concentrations: 0 (*solid thick line*), 15 (*solid thin line*), 25 (*dashed line*), 45 (*dash-dot-dot-dash line*), and 65 (*dotted line*) % v/v. (*Upper* and *lower panels*) Far- and near-UV CD spectra are shown, respectively. (*Insets*) For the sake of comparison, near-UV CD spectra corresponding to 25, 45, and 65% v/v TFE are shown.

By contrast, a dramatic red shift (9 nm) occurs between 20 and 25% v/v TFE and, from that point up to the highest concentration assayed (70% v/v), an additional 5-nm red shift is observed. The integrated intensity remains rather constant from 20 up to 45% v/v TFE only to gradually decrease by approximately fivefold at 70% v/v with respect to the initial value. An overall similar trend is observed in the intensity and shift of $\lambda_{max}$ measured for Δ98Δ.

Nonetheless, in this case one should note the following:

1. a 1.5-fold enhancement in fluorescence intensity occurs upon addition of as little as 5% v/v TFE, before starting the overall descending trend, and
2. most significantly, an abrupt increase in $\lambda_{max}$, albeit of a smaller magnitude (4 nm) by comparison with IFABP, takes place in the same TFE range (20–25% v/v) as the wild-type protein.

Because the excitation wavelength (295 nm) falls close to the edge of the absorption of Trp, we checked the invariance of the intensity-normalized excitation spectra for each protein at TFE concentrations in the range 0–60% v/v (see Fig. S3). Altogether, in agreement with results from CD measurements, the evidence derived from the fluorescence quenching of Trp residues does not suffice to account for the above observations, revealing the occurrence of conformational changes as well.

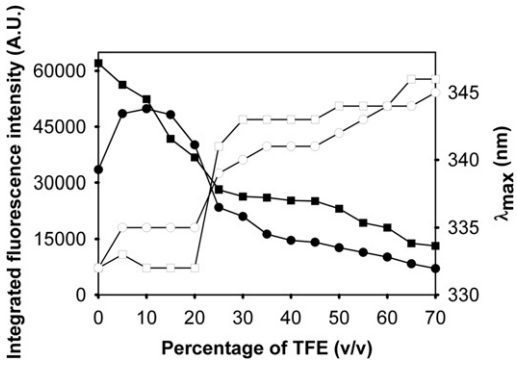


FIGURE 10 Fluorescence spectroscopy of proteins. Integrated intensity (*solid symbols*) and position of the maximum wavelength of emission ($\lambda_{max}$, *open symbols*) at the indicated concentrations of TFE are shown for IFABP (■, □) or Δ98Δ (●, ○).

## DISCUSSION

The main consequences of TFE addition on the conformation of IFABP and Δ98Δ can be analyzed from the information presented in Figs. 9 and 10. Low concentrations of TFE (i.e., $\leq$15% v/v) brings about hardly any change on the conformation of IFABP, as attested by the preservation of secondary structure and the minimal changes in tertiary structure, evidenced by the CD spectra and the unaffected fluorescence $\lambda_{max}$. The observed 33% reduction in the emission intensity is a predictable consequence of a general TFE quenching effect (26,27). For higher cosolvent concentrations, this phenomenon does not suffice to explain the observations. The onset of turbidity (Fig. 2) and the evolution of CD signals (Fig. 9, *A* and *C*) reveal that further conformational changes and aggregation occur as well. Particularly at 25% v/v TFE, the structural rearrangements observed by CD spectroscopy occur concurrently with significant decreases in fluorescence intensity and red shift of $\lambda_{max}$. These results, combined with those obtained from Th-T and CR binding, and from transmission electron microscopy and optical birefringence (Figs. 6–8), provide support for the amyloidlike character of the aggregated protein. Within the range in which aggregation takes place (25–55% v/v TFE), the invariance of the fluorescence (Fig. 10) and the similarity of the CD spectra (Fig. 9, *A* and *C*) point to a common conformation for the aggregated species.

Interestingly, at 65% v/v TFE the buildup of a helix-rich form concomitant with loss of the rigid Trp environment evidences a transition to a molten globule state. In this condition, the $\lambda_{max}$ of emission is 9-nm blue-shifted with respect to unfolded IFABP in 3 M guanidinium hydrochloride (355 nm, result not shown) and 4-nm blue-shifted with respect to NATA at 100% v/v TFE. This goes in line with the existence of a somewhat solvent-occluded (albeit flexible) environment for Trp-82. Although under this condition the protein evolves into a form that remains soluble (Fig. 2), this fact does not preclude the binding of dyes commonly used for detecting amyloid fiber formation (Fig. 6). In this regard, it is well known that CR is bound by molten globules (28). In summary, the 65% v/v TFE condition leads to a nonaggregating molten globule conformation of IFABP.

The general behavior of Δ98Δ resembles that of IFABP, although the abridged protein exhibits features indicating a higher conformational plasticity. At variance with the parent protein, Δ98Δ shows a bimodal effect (Fig. 10), where the cosolvent causes a 1.5-fold increase in the fluorescence emission and a 3-nm red shift in $\lambda_{max}$ with respect to buffer alone for the range 5–15% v/v before adopting the expected descending trend. Concurrent with these changes in fluorescence, intensification of all spectral features in both far- and near-UV CD takes place, a fact indicative of structure consolidation.

One should notice that Δ98Δ preserves all the critical residues of the hydrophobic core, i.e., those involved in the nucleation event leading to the folded state. This goes in line with the proposed hierarchical folding mechanism for IFABP ((29); see also Dalessio et al. (25,30)). However, Δ98Δ would be unable to complete the final hydrogen-bonding step leading to structure consolidation. This process might lead to a nativelike topology with a compact hydrophobic core, but endowed with an expanded periphery. In this scenario, subaggregating amounts of TFE might favor an increased rigidity of Δ98Δ.

Remarkably, $\lambda_{max}$ and fluorescence intensity of Δ98Δ are very similar to those of IFABP at 25 and 45% v/v TFE (Fig. 10). In agreement with this evidence, the CD spectra of both proteins also behave similarly in this range (Fig. 9). Taken together, these data point to the akin nature of the final aggregation product. In a fashion similar to IFABP, at 65% v/v TFE Δ98Δ shows the build-up of a soluble $\alpha$-helical structure, as attested by the far-UV CD spectra (Fig. 9). This reveals a transition to a molten globule conformation, not excluding the ability to bind amyloid-staining dyes.

As regards the aggregation phenomenon studied at 25% v/v TFE, for both proteins the observed kinetics can be explained by a nucleation-elongation mechanism (see Scheme 1). The first event is a fast equilibrium step, where TFE induces a conformational rearrangement of the native protein ($P$) giving rise to an aggregation-prone state ($P^*$). The ensuing aggregation process includes the nucleation of the conformationally altered protein into a species $P^*_n$ with a defined number $n$ of subunits ($n = 2$ for both proteins assayed in this article), followed by the growth of the fibrillar aggregates ($F$) by the irreversible apposition of more monomer. This represents a minimal scheme, similar to that proposed by Watzky and Finke (32).

Given that we avoided stirring of the samples, minimal effects on this process due to fragmentation of the fibrils are expected (14). In this scenario, the lag period of the kinetics is mainly related to the nucleation stage. One can expect that increasing the protein concentration will favor the formation of the nucleus, consequently decreasing the duration of the lag period (Fig. 4 *C*). The observed dependence of $t_0$ on protein concentration is consistent with the behavior predicted by a nucleation-elongation mechanism. After completion of the nucleation stage, aggregate growth proceeds as a pseudo-first-order reaction, where the concentration of nuclei remains constant (steady-state regime). Given that the duration of the lag phase and the $A_{lim}$ are similar for both IFABP and Δ98Δ, the main difference between the proteins is that the abridged variant shows a relatively reduced rate of aggregation (Fig. 4).

A common tenet in the field is that aggregation in vitro can be favored by destabilizing the native state of the protein. There are several examples where the first critical step in fibrillogenesis is the partial unfolding of the protein (8,33,34). Due to thermal fluctuations, the average structure of a globular protein under physiological conditions can be pictured as a rapidly interconverting mixture of tightly folded and multiple partially unfolded conformations (i.e., conformational breathing), with the former greatly predominating in the population. In this regard, most mutations associated with accelerated fibrillation and protein deposition diseases have been shown to destabilize the native structure in the ensemble, thus increasing the concentration of partially folded conformers. It has been shown for several proteins that destabilization of the native globular structure (e.g., at low or high pH, high temperatures or pressure, low-to-moderate concentrations of strong denaturants or organic solvents, etc.) may significantly accelerate the rate of fibril formation (33).

Contrary to expectation, Δ98Δ displays a similar (or even lower) tendency to aggregate. In agreement with the hierarchical folding model proposed for IFABP (29), Δ98Δ would presumably complete most of the stages leading to the folded state. Thus, by its very nature Δ98Δ would constitute a minimalist model capable of populating conformations scarcely represented in the ensemble of the full-length protein (2). In fact, evidence for equilibrium intermediates in IFABP structurally akin to Δ98Δ has already been reported by NMR (35,36). In this context, Δ98Δ would emerge as a useful model to study aggregation propensity of $\beta$-barrel proteins.

Being an abridged form of IFABP able to adopt a nativelike topology, the Δ98Δ framework becomes useful for

interrogating those structural determinants of IFABP related to aggregation. However, the current view holds that aggregation propensity might be the function of relatively short sequences (37). Although peptide 1–28 in the context of the full structure includes the most flexible regions of the protein, this characteristic alone does not grant it the ability to act as a core for aggregation. By itself or in the presence of Δ98Δ, this peptide does not form aggregates (Fig. 3). In addition, this peptide behaves as an unstructured entity in isolation, evolving into a helical structure if challenged with 25 v/v % TFE. Significantly, regardless of the presence of TFE, the spectrum of the 1:1 mixture of Δ98Δ and peptide 1–28 is indistinguishable from the algebraic sum of spectra corresponding to each isolated moiety (see Fig. S4).

Nevertheless, the above mixing experiments do not rule out the possibility that interactions between the N-terminal moiety and the main central region might be too weak to be observed even at the highest peptide and protein concentrations assayed. As a cautionary note, one should be aware that the overall aggregation propensity of a given construct may not be only a function of a local amino-acid sequence, because interactions between different regions might also play an important role in the process. Because mutations on the segments implicated in the last event of the hierarchical folding scheme have profound effects on the structure and stability of the constructs (38–40), it cannot be ruled out that in the context of the protein, unless those residues attain the precise conformation present in the native form, they could contribute to the aggregation propensity observed for the full-length protein. Δ98Δ lacks both the N- and C-terminal stretches, which mutually interact to complete the last step in the folding of the $\beta$-barrel.

Despite leading to a less stable structure, the extensive truncation yields a folded and flexible form exhibiting a somewhat lower tendency to aggregate. This paradoxical finding appears at odds with the notion that the perturbation of the native compact fold would inescapably populate aggregation-prone species.

## SUPPORTING MATERIAL

Four figures are available at http://www.biophysj.org/biophysj/supplemental/S0006-3495(12)01014-4.

The authors thank Ms. Inés Cabanas for her collaboration with the purification of proteins, Mr. Santiago M. Delfino for his assistance with light microscopy photographs, and Dr. Mariano González Lebrero for his help with rendering Fig. 1.

This research has been supported by grants to J.M.D. and L.M.C. from the University of Buenos Aires (UBACyT Nos. B-901 and IJ-069), the Consejo Nacional de Investigaciones Científicas y Técnicas (CONICET PIP No. 1936), and the Agencia Nacional de Promoción Científica y Tecnológica (ANPCyT PICT Nos. 2007-0632 and 2010-0460). C.R.A. has been awarded an undergraduate student fellowship from the University of Buenos Aires. L.M.C., J.J.C., and J.M.D. hold teaching positions at the University of Buenos Aires and are career researchers of CONICET.

## REFERENCES

1. Curto, L. M., J. J. Caramelo, and J. M. Delfino. 2005. Δ98Δ, a functional all-$\beta$-sheet abridged form of intestinal fatty acid binding protein. *Biochemistry.* 44:13847–13857.
2. Curto, L. M., J. J. Caramelo, …, J. M. Delfino. 2009. Δ98Δ, a minimalist model of antiparallel $\beta$-sheet proteins based on intestinal fatty acid binding protein. *Protein Sci.* 18:735–746.
3. Franchini, G. R., L. M. Curto, …, J. M. Delfino. 2009. Dissection of a $\beta$-barrel motif leads to a functional dimer: the case of the intestinal fatty acid binding protein. *Protein Sci.* 18:2592–2602.
4. Richardson, J. S., D. C. Richardson, …, M. E. Donlan. 1992. Looking at proteins: representations, folding, packing, and design. Biophysical Society National Lecture, 1992. *Biophys. J.* 63:1185–1209.
5. Quinn, T. P., N. B. Tweedy, …, D. C. Richardson. 1994. Betadoublet: de novo design, synthesis, and characterization of a $\beta$-sandwich protein. *Proc. Natl. Acad. Sci. USA.* 91:8747–8751.
6. Richardson, J. S., and D. C. Richardson. 2002. Natural $\beta$-sheet proteins use negative design to avoid edge-to-edge aggregation. *Proc. Natl. Acad. Sci. USA.* 99:2754–2759.
7. Hong, D., M. Hoshino, …, Y. Goto. 1999. Clustering of fluorine-substituted alcohols as a factor responsible for their marked effects on proteins and peptides. *J. Am. Chem. Soc.* 121:8427–8433.
8. Chiti, F., and C. M. Dobson. 2009. Amyloid formation by globular proteins under native conditions. *Nat. Chem. Biol.* 5:15–22.
9. Calamai, M., G. G. Tartaglia, …, C. M. Dobson. 2009. Mutational analysis of the aggregation-prone and disaggregation-prone regions of acylphosphatase. *J. Mol. Biol.* 387:965–974.
10. Chiti, F., N. Taddei, …, C. M. Dobson. 2000. Mutational analysis of the propensity for amyloid formation by a globular protein. *EMBO J.* 19:1441–1449.
11. Gast, K., D. Zirwer, …, G. Damaschun. 1999. Trifluoroethanol-induced conformational transitions of proteins: insights gained from the differences between $\alpha$-lactalbumin and ribonuclease A. *Protein Sci.* 8:625–634.
12. Rezaei-Ghaleh, N., A. Ebrahim-Habibi, …, M. Nemat-Gorgani. 2007. Role of electrostatic interactions in 2,2,2-trifluoroethanol-induced structural changes and aggregation of $\alpha$-chymotrypsin. *Arch. Biochem. Biophys.* 457:160–169.
13. Arighi, C. N., J. P. F. C. Rossi, and J. M. Delfino. 2003. Temperature-induced conformational switch in intestinal fatty acid binding protein (IFABP) revealing an alternative mode for ligand binding. *Biochemistry.* 42:7539–7551.
14. Knowles, T. P., C. A. Waudby, …, C. M. Dobson. 2009. An analytical solution to the kinetics of breakable filament assembly. *Science.* 326:1533–1537.
15. Nilsson, M. R. 2004. Techniques to study amyloid fibril formation in vitro. *Methods.* 34:151–160.
16. Schmid, F. 1989. Spectral methods of characterizing protein conformation and conformational changes. *In* Protein Structure: a Practical Approach. T. E. Creighton, editor. IRL, New York. 251.
17. Flyvbjerg, H., E. Jobs, and S. Leibler. 1996. Kinetics of self-assembling microtubules: an "inverse problem" in biochemistry. *Proc. Natl. Acad. Sci. USA.* 93:5975–5979.
18. Wang, K., and B. I. Kurganov. 2003. Kinetics of heat- and acidification-induced aggregation of firefly luciferase. *Biophys. Chem.* 106:97–109.
19. LeVine, 3rd, H. 1993. Thioflavine T interaction with synthetic Alzheimer's disease $\beta$-amyloid peptides: detection of amyloid aggregation in solution. *Protein Sci.* 2:404–410.
20. Pallarès, I., J. Vendrell, …, S. Ventura. 2004. Amyloid fibril formation by a partially structured intermediate state of $\alpha$-chymotrypsin. *J. Mol. Biol.* 342:321–331.
21. Whitmore, L., and B. A. Wallace. 2004. DICHROWEB, an online server for protein secondary structure analyses from circular dichroism spectroscopic data. *Nucleic Acids Res.* 32(Web Server issue):W668–W673.

22. Whitmore, L., and B. A. Wallace. 2008. Protein secondary structure analyses from circular dichroism spectroscopy: methods and reference databases. *Biopolymers.* 89:392–400.

23. Andrade, M. A., P. Chacón, …, F. Morán. 1993. Evaluation of secondary structure of proteins from UV circular dichroism spectra using an unsupervised learning neural network. *Protein Eng*. 6:383–390.

24. Arighi, C. N., J. P. F. C. Rossi, and J. M. Delfino. 1998. Temperature-induced conformational transition of intestinal fatty acid binding protein enhancing ligand binding: a functional, spectroscopic, and molecular modeling study. *Biochemistry.* 37:16802–16814.

25. Dalessio, P. M., S. E. Fromholt, and I. J. Ropson. 2005. The role of Trp-82 in the folding of intestinal fatty acid binding protein. *Proteins.* 61:176–183.

26. Chen, Y., B. Liu, and M. D. Barkley. 1995. Trifluoroethanol quenches indole fluorescence by excited-state proton transfer. *J. Am. Chem. Soc*. 117:5608–5609.

27. Mukhopadhyay, K., and S. Basak. 1998. Conformation induction in melanotropic peptides by trifluoroethanol: fluorescence and circular dichroism study. *Biophys. Chem*. 74:175–186.

28. Khurana, R., V. N. Uversky, …, A. L. Fink. 2001. Is Congo Red an amyloid-specific dye? *J. Biol. Chem*. 276:22715–22721.

29. Yeh, S. R., I. J. Ropson, and D. L. Rousseau. 2001. Hierarchical folding of intestinal fatty acid binding protein. *Biochemistry.* 40:4205–4210.

30. Dalessio, P. M., J. A. Boyer, …, I. J. Ropson. 2005. Swapping core residues in homologous proteins swaps folding mechanism. *Biochemistry.* 44:3082–3090.

31. Reference deleted in proof.

32. Watzky, M. A., and R. G. Finke. 1997. Transition metal nanocluster formation kinetic and mechanistic studies. A new mechanism when hydrogen is the reductant: slow, continuous nucleation and fast autocatalytic surface growth. *J. Am. Chem. Soc*. 119:10382–10400.

33. Uversky, V. N., and A. L. Fink. 2004. Conformational constraints for amyloid fibrillation: the importance of being unfolded. *Biochim. Biophys. Acta*. 1698:131–153.

34. Silva, J. L., and D. Foguel. 2009. Hydration, cavities and volume in protein folding, aggregation and amyloid assembly. *Phys. Biol*. 6:015002.

35. Hodsdon, M. E., and C. Frieden. 2001. Intestinal fatty acid binding protein: the folding mechanism as determined by NMR studies. *Biochemistry.* 40:732–742.

36. Ropson, I. J., J. A. Boyer, and P. M. Dalessio. 2006. A residual structure in unfolded intestinal fatty acid binding protein consists of amino acids that are neighbors in the native state. *Biochemistry.* 45:2608–2617.

37. Pawar, A. P., K. F. Dubay, …, C. M. Dobson. 2005. Prediction of "aggregation-prone" and "aggregation-susceptible" regions in proteins associated with neurodegenerative diseases. *J. Mol. Biol*. 350: 379–392.

38. Kim, K., and C. Frieden. 1998. Turn scanning by site-directed mutagenesis: application to the protein folding problem using the intestinal fatty acid binding protein. *Protein Sci*. 7:1821–1828.

39. Clérico, E. M., S. G. Peisajovich, …, M. R. Ermácora. 2000. Engineering a compact non-native state of intestinal fatty acid-binding protein. *Biochim. Biophys. Acta*. 1476:203–218.

40. Chattopadhyay, K., S. Zhong, …, C. Frieden. 2002. The intestinal fatty acid binding protein: the role of turns in fast and slow folding processes. *Biochemistry.* 41:4040–4047.